Synthesis and characterization of heteropolyacid nanoporous carbon membranes

Michael S. Strano [a] and Henry C. Foley [b,*]

[a] *Department of Chemical Engineering, University of Delaware, Colburn Laboratory, Academy Street, Newark, DE 19716, USA*
E-mail: strano@che.udel.edu
[b] *Head, Department of Chemical Engineering, Pennsylvania State University, University Park, PA 16802, USA*

Received 22 February 2001; accepted 19 April 2001

Heteropolyacid nanoporous carbon membranes were synthesized by re-precipitation of 12-tungstophosphoric acid on a prefabricated nanoporous carbon film. The Keggin structure is maintained on and within the 8 μm film as inferred from FTIR spectroscopy and XRD. Gas permeation reveals that separation performance of the carbon membrane is maintained after deposition although total membrane flux decreases by nearly 40% for N_2 permeation. Semi-batch membrane reactor performance in the decomposition of methyl *tert*-butyl ether at 55 °C shows significant enhancement of the conversion with 96.5% compared with 64.1% for a non-selective membrane analog under the same conditions.

KEY WORDS: heteropolyacids; membrane reactors; MTBE decomposition; isobutylene production

1. Introduction

Catalytic membrane reactors have attracted the attention of many researchers in an effort to improve existing catalytic processes through combined reaction and selective permeation [1–3]. Armor [4] emphasizes the need to develop membranes using highly selective materials for use as catalytic reactors, observing that catalysts with larger pores and low transport selectivity still require downstream separation to recover the product of value. Reports using zeolite-based membranes as inert (non-catalytic) membrane reactors [5–7] have shown small increases in reactor conversion or separation efficiency of reactants and products. Itoh and Haraya, however, have been able to demonstrate considerable conversion enhancement by nearly a factor of 2 in the dehydrogenation of cyclohexane to benzene using a nanoporous carbon membrane reactor [8].

While these studies have utilized inert membrane reactors – reactors where the catalyst exists externally from the selective membrane barrier – there are advantages in utilizing a membrane catalyst. These include the elimination of mass transfer resistance at the surface and in the bulk of the catalyst particle, as well as decreased overall reactor volumes. Such improvements are referred to as process intensification. The first such catalytic, nanoporous membrane demonstrated in the literature utilizes molecular sieving or nanoporous carbon (NPC) supported on stainless steel and rendered catalytic by incorporation of Pt into the film [9]. Formed from the pyrolysis of non-graphitizing natural or synthetic polymeric precursors, NPC is a disordered carbon material having pores on the scale of molecular dimensions and has been shown to generally possess "shape selective" molecular transport properties [10].

Nanoporous carbon (NPC) is a promising material for use as a catalytic membrane in that it is chemically inert under most reaction conditions and thermally stable at temperatures well above 200 °C where most industrially relevant reactions occur [11]. Polyfurfuryl alcohol (PFA) derived nanoporous carbons have a mean pore size about 0.5 nm as measured from N_2 and methyl chloride adsorption isotherms [12]. Membranes have been fabricated using NPC that are selective for the separation of small molecular species [13–15]. Films of nanoporous carbon have also been synthesized with some of the highest ideal selectivity values reported in the literature for O_2/N_2 and He/O_2 separation [15].

Heteropolyacids (HPAs) have both redox and acid catalytic properties and have been used as catalysts in several commercialized processes such as propylene [16] and isobutylene hydration [17]. Porous carbons have been demonstrated as excellent supports for HPA catalysts [18], although the nature of catalyst adsorption into the carbon pores is poorly understood [19]. Schwegler *et al.* [19] have explored the synthesis of activated carbon supported phosphotungstic and silicotungstic acid catalysts and have suggested that chemical adsorption of the HPA involves proton transfer to the carbon surface. Lee *et al.* [20,21] have used silica-supported $H_3PW_{12}O_{40}$ packed externally from various polymer membranes and have shown selectivity and conversion enhancement in the low temperature decomposition of methyl *tert*-butyl ether (MTBE). The membranes utilized were selective towards the permeation of methanol over isobutylene and MTBE. The authors were able to use this characteristic to demonstrate increases as high as 10%

* To whom correspondence should be addressed.

1011-372X/01/0700-0177$19.50/0

in conversion at 100 °C [21] over a conventional plug-flow reactor as well as a 97% methanol purity in the permeate stream [20].

In this study, a novel form of heteropolyacid carbon membrane has been synthesized by precipitation of $H_3P_{12}O_{40}$ from a methanol solution onto a prefabricated nanoporous carbon membrane. The composite catalytic membrane system retains the shape selective transport properties of the nanoporous carbon film and the acid and redox catalytic activity of the heteropolyacid over-layer. The membranes are characterized by scanning electron microscopy, FTIR spectroscopy, XRD and the permeation of low molecular weight gases at 298 K. The selective permeation properties are benchmarked against a non-selective porous graphite film in the decomposition of MTBE in a semi-batch membrane reactor held isothermal at 55 °C.

2. Membrane synthesis

Nanoporous carbon membranes were synthesized by spray deposition followed by pyrolysis of poly(furfuryl alcohol) (Monomer Polymer and Dajac Laboratories Inc., Lot A-1-143) on 316 sintered metal stainless-steel supports (0.2 μm pore size, 11.4 cm^2 area) obtained from Mott Metallurgical Co. Detailed descriptions of the synthesis method [14] and characteristics [13] for these nanoporous carbon membranes appear elsewhere. The temperature history of the pyrolysis was a 5 °C/min ramp to 600 °C and held for 2 h. The carrier gas utilized was dry, de-oxygenated He at 50 sccm. The completed membranes were separately added to 50 ml of 10 mg/ml solution of 12-tungstophosphoric acid, $H_3PW_{12}O_{40}$, (PW) hydrate (Sigma Aldrich) used without further purification. The solvent was allowed to evaporate entirely at 298 K under stirring after which time the membranes were removed, washed in a stream of methanol and dried in a vacuum furnace at 100 °C under 3 Torr vacuum overnight. Catalytic loading in the range of 1 mg/m^2 was inferred from a combination of scanning electron microscopy and elemental analysis detailed below. A "non-selective" carbon membrane was fabricated for comparison purposes using two circular, non-porous graphite disks of 1 cm thickness punched from readily available sheet material (McMaster-Carr). A 0.3 mm diameter wire was used to punch ten off-center holes through both disks. The surface of one was rendered catalytic using the same procedure outlined above. Both disks were subsequently pressed together in the stainless-steel reactor module described below.

3. Characterization

3.1. SEM imaging and elemental analysis of membrane surfaces

Membranes were cut with a diamond wafering saw and the cross sections were mounted in epoxy for imaging with a Hitachi S-4000 field emission scanning electron microscope. Images of external membrane surfaces were also obtained. Qualitative elemental analysis was performed with an Elmer 9900 EDAX at 20 keV to verify the existence or non-existence of a measurable W cross section of a given surface.

3.2. Powder X-ray diffraction

Carbon material was removed from the stainless-steel support using a surgical scalpel and mounted for X-ray diffraction using an X'Pert model auto-sampling diffractometer with a Cu K_α radiation source at 45 keV and 40 mA.

3.3. FTIR spectroscopy

Keggin type heteropolyacids in particular have a distinct FTIR signature corresponding to their primary and secondary structure. The PW/C material was removed from the stainless-steel support and combined with KBr to make a 1% mixture. These samples were then pressed into translucent pellets and mounted for adsorption spectral analysis using an Infinity series ATI Mattson FTIR spectrometer.

3.4. Single component gas permeability

Permeation of He, N_2, O_2 , Ar, CO_2 and SF_6 was used to characterize the selective porosity and integrity of each catalytic carbon membrane. The disk-shaped membranes were sealed using Viton™ gaskets coated with a small amount of silicone vacuum grease into a stainless-steel module set up to measure the transport of a single gas through the membrane. The apparatus and method are described elsewhere [22]. The flux of each gas was measured as a function of driving force pressure applied to each of the catalytic membranes. Testing was performed on both prefabricated carbon membranes and samples after catalytic deposition.

3.5. Decomposition of methyl tert-butyl ether

Catalytic membranes were tested for the decomposition of MTBE using a semi-batch equilibrium membrane reactor depicted in figure 1. The catalytic membrane was sealed into a stainless-steel module using Viton™ gaskets (MDC Vacuum products) with the catalytic surface facing in towards the enclosed chamber as shown. This chamber was purged with dry, de-oxygenated Ar before reaction. The membrane reactor setup was held isothermal at 55 °C by enclosing the entire module into a 2000 ml heating mantle (Ace Glass Inc.) with an insulated cover.

At a time $t = 0$, a volume of liquid MTBE metered using a micro-syringe (0–100 μl) was injected into the enclosed chamber above the surface of the membrane. The pressure was allowed to reach a maximum and the product fluxes permeating through the opposing face of the membrane were carried from the reactor using an Ar sweep gas

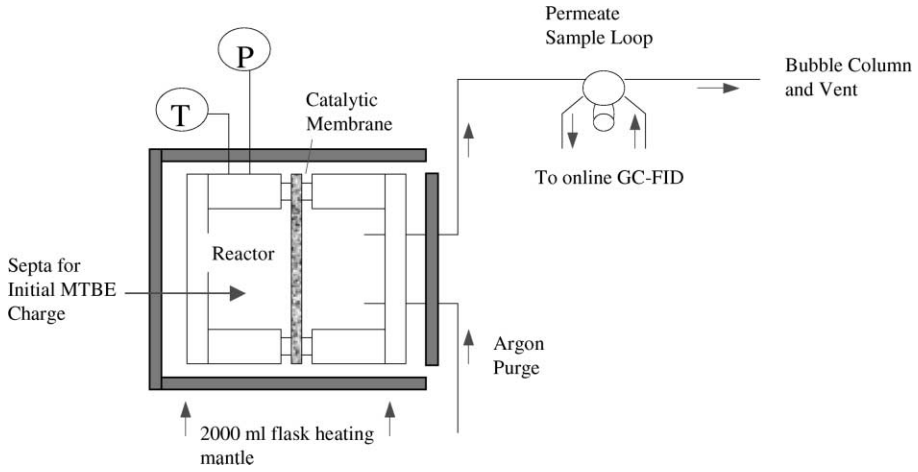

Figure 1. Diagram of semi-batch catalytic membrane reactor setup.

flowing at 10 sccm. This stream was analyzed every 15 min using a Varian 3700 gas chromatograph with an FID detector and a Porapak Q column (0.25″ OD, 4′ long, held at 160 °C isothermal, 50 sccm Ar carrier, 40 psig total pressure). The largest molecular species of the anticipated gas phase products, diisobutylene possessed a retention time of 12.8 min using these column conditions, with 0.4 min in separation between dimethyl ether (DME) and methanol. Where indicated, a Porapak N column was used to affect greater DME/methanol peak resolution. A mass balance was performed using the known injected MTBE amount, the final concentrations remaining in the enclosed volume and the time integrated fluxes from the permeate side. This conversion was checked against the material balances for the product distribution based upon methanol and isobutylene.

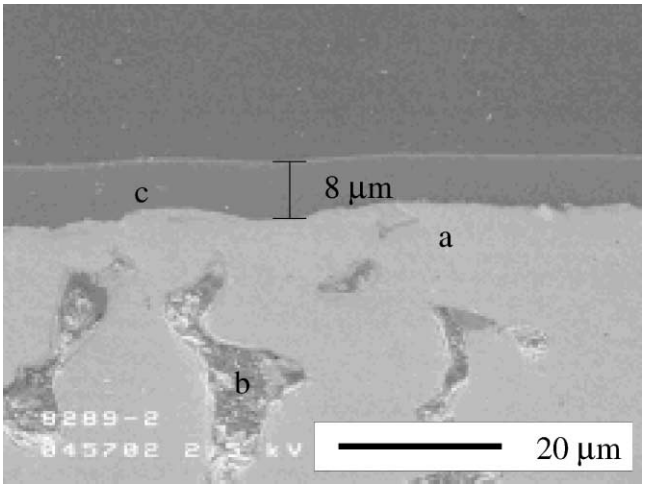

Figure 2. Scanning electron micrograph of membrane cross section (orthogonal to membrane surface). **a** stainless-steel support, **b** 10 μm support pore and **c** carbon layer.

4. Results and discussion

4.1. Scanning electron microscopy and elemental analysis

Figure 2 is the cross section of a catalytic membrane with a carbon layer of about 8 μm thickness visible above the porous stainless steel and is typical for supported membranes of this type [13]. Elemental measurements centered about the membrane cross sections as shown failed to yield a detectable W cross section on all samples, indicating that catalyst concentrations within the carbon film were less than about 0.1 wt% over an averaged 500 nm × 500 nm area. Figure 3 is an image taken above the membrane external surface showing TPA domains coalesced upon the external surface. EDAX performed on the external surfaces of impregnation type membranes was able to detect W as well as Fe lines. Estimating each anchored crystallite as spherical, the total volume density from a series of such micrographs is about 0.003 cm^3 of TPA hydrate/m^2 of membrane and the mode in the distribution of crystallite diameters is approximately 60 nm.

4.2. FTIR spectroscopy

The FTIR spectra of membrane material (figure 4) show preservation of the Keggin structure with characteristic bands at 794 and 892 corresponding to the νW–O–W groups (edge and corner, respectively) and those at 984 and 1080 each representing νW=O and νP–O, respectively. Schwegler *et al.* [19] report an unexplained, slight shifting of the Keggin peaks to higher wavenumbers for activated carbon/PW materials. The lack of wavenumber shift or peak splitting may suggest little chemical interaction between the PW with the carbon surface. This is consistent with a nucleation and growth type mechanism where crystallites initially physically adsorb in larger surface irregularities and cracks on the membrane surface, as also suggested by SEM surface images. The broadening of the band at 595 cm^{-1} (corresponding to δO–P–O) for the catalytic membrane sample is partially remnant of the original carbon film as shown.

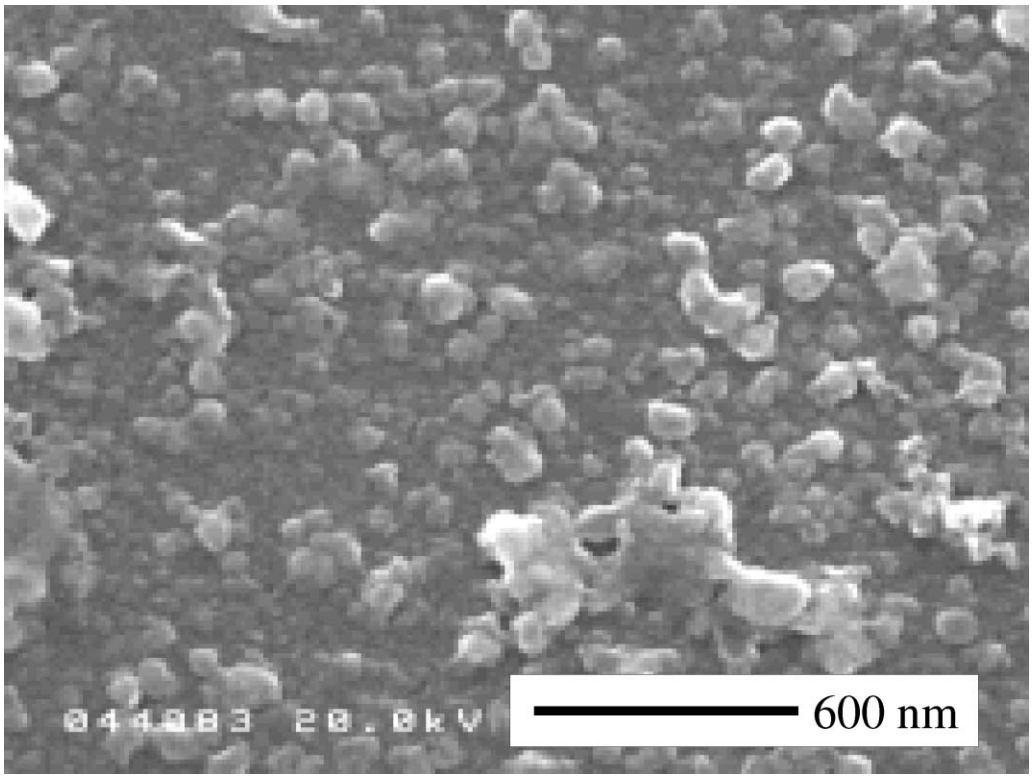

Figure 3. Scanning electron micrograph of external membrane surface showing excess 12-tungstophosphoric acid crystallites dispersed on the carbon surface.

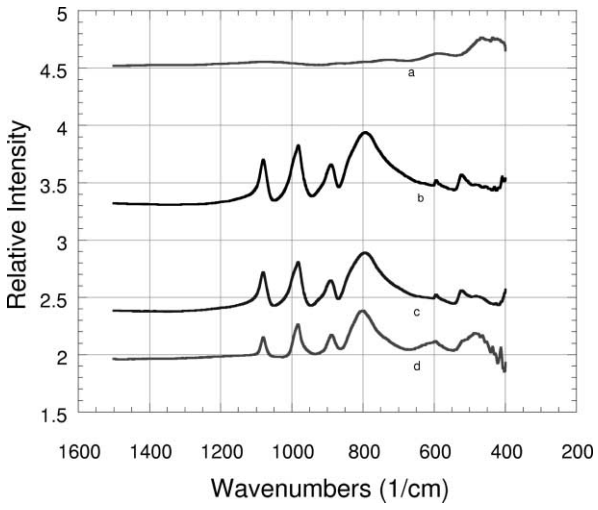

Figure 4. FTIR spectra of the 400–1300 1/cm region for (a) PFA carbon synthesized at 600 °C, (b) PW, (c) 50% PW/C physical mixture and (d) PW/NPC membrane material.

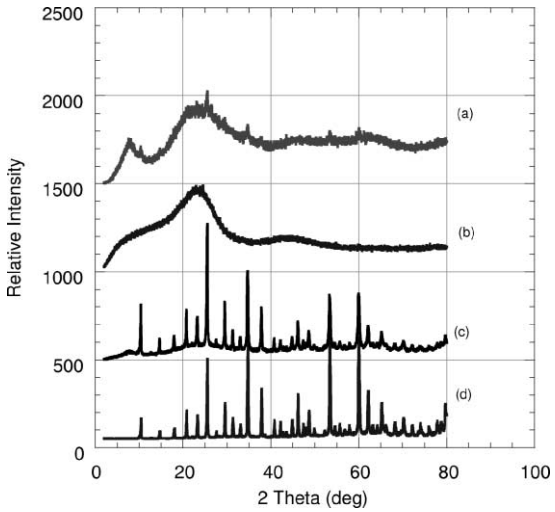

Figure 5. XRD patterns from 2° to 80° 2θ for (a) PW/NPC membrane material, (b) PFA carbon synthesized at 600 °C, (c) 50% PW/C physical mixture and (d) PW hydrate.

4.3. Powder X-ray diffraction

Figure 5 presents the XRD patterns of a catalytic membrane before and after impregnation as well as PW and a 50% PW/C physical mixture for comparison. The catalytic membranes show a retention of diffraction features for both primary and secondary PW structure at ambient temperature. This indicates that PW dispersion is significantly lower than that produced on larger pore carbons, which characteristically demonstrate no diffraction pattern contribution of PW even at loading as high as 25% [23]. Nanoporous carbons, which are largely amorphous, typically have a broad diffraction peak at 22° 2θ with a smaller peak at 44°. Crystalline graphite has sharp, prominent peaks near these locations. The curious broad diffraction peak at 8° 2θ appears consistently in PW/carbon membrane patterns. The peak is absent from the pattern for unsupported PW (figure 6) as well as that of PFA carbon. The feature may arise from physical adsorption

of smaller PW domains within the limited mesoporosity of the carbon film. Similar PW impregnation of MCM-41 has been shown to distort small angle XRD features in an analogous manner [24]. Previous studies of TPA on activated carbon unfortunately present no detailed diffraction information of the carbon support in the low angle diffraction region from which to discern similar catalyst/carbon interactions in XRD spectra [23].

4.4. Single component gas permeability

Figure 6 compares the single component gas fluxes through both a PW/NPC membrane and non-selective graphite membrane analog. The former demonstrates a linearity in flux *versus* pressure for He, O_2, Ar and N_2 as seen for inert catalytic nanoporous membranes. The O_2/N_2 flux ratio (3.4) is higher than the Knudsen value (0.94) and is indicative of nanopore dominated transport across the film. Stronger adsorbing gases, CO_2 and SF_6, show a saturation type behavior as evidenced by a slope less than unity. The porous graphite disk by contrast shows very little permselectivity between gases. The slope on a log–log plot of flux *versus* pressure of approximately two suggests a quadratic dependence of flux *versus* pressure indicative of viscous flow and Knudsen transport mechanisms.

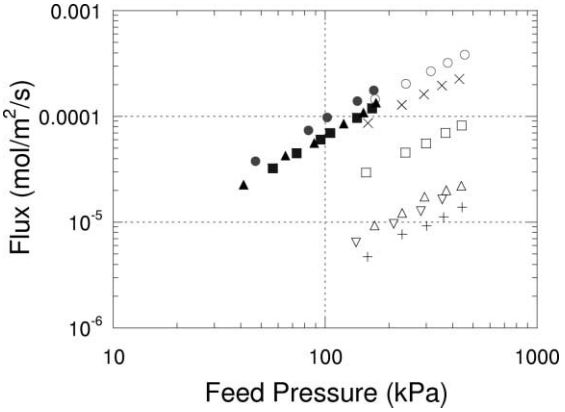

Figure 6. Fluxes of single component, inert gases through PW/NPC membrane (empty symbols) and porous graphite disk (filled symbols): (□, ■) O_2, (∇) Ar, (+) SF_6, (×) CO_2, (△, ▲) N_2 and (○, ●) He.

Both single component membrane permeabilities and individual permselectivities decrease after deposition. The N_2 permeance of 5.5×10^{-11} mol/m^2 s Pa falls to 3.53×10^{-11} mol/m^2 s Pa after deposition. Similarly the He value of 8.5×10^{-10} decreases to 3.5×10^{-10} mol/m^2 s Pa. This corresponds to an ideal selectivity reduction from 15.3 to 11.8. A similar reduction in selectivity has been observed by Strano and Foley for inert carbon membranes [25] where heating of the film under vacuum at 150 °C reduced He/N_2 selectivity by 53%. This reduction was attributed to the removal of adsorbed gases formed during the initial pyrolysis of the film as it was observed to be irreversible after the initial heat treatment. Subsequent measurements were reproducible over the range from 298 to 498 K. After evacuation of adsorbed gases, however, membrane permeances increase while the opposite trend is observed in the case of the catalytic system in this work. The decrease in fluxes after catalytic deposition is likely due to the mass transport resistance of the catalytic layer, which has been observed to be itself microporous and hence is expected to contribute to membrane resistance. Nanoscale characterization of $H_3P_{12}O_{40}$ deposited on highly ordered pyrolytic carbon has shown the formation of ordered arrays with 1.17 ± 0.01 nm periodicity [26]. Such a structure, albeit disordered in the case of composite PW/NPC membranes, would limit the available external carbon area for transport.

4.5. MTBE decomposition

Figure 7 (a) and (b) shows the product fluxes from both a PW/NPC membrane and porous graphite disk after a 50 μl of MTBE injected at $t = 0$ min. Injections of 5, 30 and 100 μl of MTBE were also performed. The PW/NPC

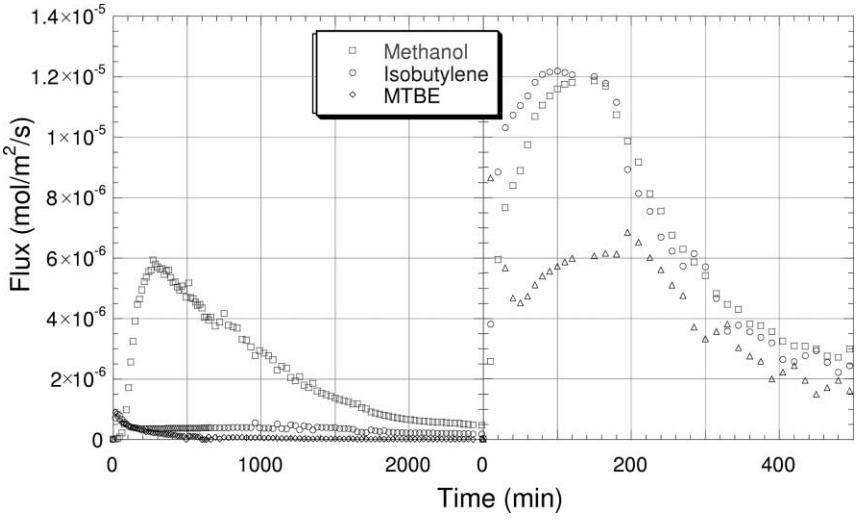

Figure 7. Product flux distributions after 50 mml injection at $t = 0$: (a) PW/NPC membrane, (b) non-selective, porous graphite disk.

membrane response is characterized by a rapid increase in the methanol flux to a maximum presumably as the membrane attains steady state followed by a broad decay as MTBE is consumed within the catalytic membrane and the driving force subsequently decreases. The maximum in methanol flux is nearly proportional to the injected reactant volume with 1.0×10^{-5}, 5.7×10^{-6}, 3.6×10^{-6} and 6×10^{-7} mol/m^2 s for 100, 50, 30 and 5 μl injections, respectively. Each occurs between about 200 and 280 min after injection. The isobutylene and MTBE fluxes also show characteristic trends with isobutylene increasing rapidly initially followed by a subsequent decay. This decay is even more rapid for MTBE, which apparently reaches a maximum in less than 15 min. The behavior is similar to that for gas mixtures through other types of nanoporous membranes where there is a transient displacement of components with weaker extents of adsorption. The membrane apparently suppresses transport of the MTBE and to a lesser extent isobutylene in favor of the faster permeating methanol. Reactor conversions based on MTBE are quite high with 84.4, 93.3, 96.5 and 98.3% each corresponding 5, 30, 50 and 100 μl injections, respectively.

The reactor results using the non-selective graphite membrane show a membrane flux with appreciable quantities of all three primary products. The transient behavior is complex with an initial escape of unreacted MTBE reaching a maximum of 1.85×10^{-5} mol/m^2 s at 20 min followed by a significant decrease as methanol and isobutylene fluxes increase. Secondary products are not produced in significant quantities as no DME was detected and the isobutylene and methanol fluxes are nearly equal throughout the reactor cycle. The conversion as measured from MTBE balance is 64.1% for this 50 μl injection.

Comparison of the reactor performance with equilibrium conditions is difficult in that there is a lack of low temperature decomposition data available, and none with conditions near equilibrium. Chemical reaction equilibrium calculations based upon literature enthalpies and entropies of reaction (table 1) yield predominately secondary products at 55 °C and 0.3 atm total pressure.

Equilibrium compositions under these conditions are only 2.0, 0.15 and 3.1% for methanol, isobutylene and MTBE with significant quantities of dimethyl ether and diisobutylene formed. Lee *et al.* [20,21] who have studied low temperature MTBE decomposition over silica-supported PW in an inert polymer membrane reactor do not report any diisobutylene formation either directly as an on-stream component or indirectly as catalyst deactivation. Dimethyl ether (DME) production was reported as slight. This latter observation is expected for a methanol selective membrane. Since the methanol partial pressure never reaches appreciable levels in a reactor that transports this product away rapidly, methanol coupling is expected to be suppressed. A 50 μl direct injection of methanol to the reactor confirms that DME flux was less than 0.025% with a maximum in the methanol flux of 1.3×10^{-5} mol/m^2 s occurring at 25 min. The non-selective sample also does not show appreciable levels of secondary product formation in the permeate fluxes, and this is confirmed by the observation that methanol and isobutylene are produced in nearly equimolar quantities as a function of time. The same argument can be made in this case, as the maxima in methanol flux between the two membranes are close in value, 1.3×10^{-5} mol/m^2 s for the former and 1.2×10^{-5} mol/m^2 s for the latter.

Neither membrane produces measurable quantities of diisobutylene or *tert*-butyl alcohol in the permeate stream. The former, being a branched C_8 olefin, is not expected to have an appreciable flux through a nanoporous membrane of this type, which separates molecular species based roughly on molecular size. Spot checks throughout the run consisting of sampling from the top of the reactor using a gas tight syringe do not detect this component in the gas phase above the membrane. There is little evidence for irreversible adsorption or condensation of this component on the membrane itself, as neither deactivation of the catalyst nor fouling of the membrane is detectable after multiple runs through the catalytic membrane. Vaughan *et al.* [28] report appreciable oligomerization of propene over a PW type catalyst at much higher pressures of 5 MPa and at 220–230 °C. The lack of vapor phase diisobutylene observed is also consistent with the results of Lee *et al.* [20,21]. In the case of the non-selective membrane, isobutylene flux is nearly two orders of magnitude higher than in the former case and its residence time is hence lower. Formation of *tert*-butyl alcohol is suppressed in both cases by the lack of DME coupling, which provides the water necessary for hydration.

Despite the lack of experimental data for comparison, estimates can be made on the equilibrium limitations of the primary reaction. Neglecting the secondary products, catalytic membranes can be benchmarked against the integrated yield of a non-selective, semi-batch membrane reactor that transports MTBE and its primary decomposition products from the reactor at the composition of the reactor at that time. A simple expression for the integral reactor conversion as a function of initial MTBE charge pressure is derived in the appendix. The equilibrium constant as a func-

Table 1
Thermodynamic values for MTBE decomposition and secondary reactions [27].

Reaction	ΔH_{rxn} (kJ/mol)	ΔS_{rxn} (J/mol K)	$\Delta C_{p_{rxn}}$ (J/mol K)	Δn_{rxn}
MTBE → isobutylene + methanol	65.3	180.3	−1.8	1
2 isobutylene → diisobutylene	−77	−167.5	1.2	−1
2 methanol → dimethyl ether + water	−22.6	−23.4	11.8	0
water + isobutylene → *tert*-butyl alcohol	−54	−156	−10.1	−1

tion of temperature for MTBE formation from isobutylene and methanol has been computed by Lisal *et al.* [29] and a value of 18.2 bar^{-1} is obtained for 55 °C. Using this in equation (A.1) yields 74.3, 67.1, 57.6 and 90.2% for 100, 50, 30 and 5 μl MTBE injections assuming that the dilute MTBE/Ar mixture behaves ideally and using an estimated reactor volume of 43.2 cm^3. The non-selective membrane sample conversion of 64.1% is less than 67.1% at 50 μl. The nanoporous membrane yields conversions that are significantly higher than these estimated limiting values.

5. Conclusion

The synthesis of heteropolyacid nanoporous carbon membranes was investigated to create catalytic films with selective transport properties for use as membrane reactors. Heteropolyacid nanoporous carbon membranes were synthesized by impregnation of 12-tungstophosphoric acid on a prefabricated nanoporous carbon membrane. The method produces an intact Keggin structure as inferred from FTIR spectroscopy. Gas permeation experiments revealed that the procedure does not significantly change the separation performance of the film for small molecular separations. Total membrane flux, however, decreased by nearly 40% for N_2 after catalytic deposition. Semi-batch membrane conversions in the decomposition of MTBE to isobutylene and methanol at 55 °C and 5–100 μl initial injected volumes show significant enhancement of the conversion with a retention of MTBE and isobutylene in favor of the faster transporting methanol. Reactor conversions based on MTBE are quite high with 96.5% for a 50 μl injection. These were benchmarked against a non-selective, porous graphite membrane rendered catalytic in the same manner where the conversion was 64.1%. Hence, the catalytic membrane demonstrates a significant conversion enhancement with *in situ*, simultaneous separation.

Acknowledgement

This work was supported by the Department of Energy, Office of Basic Energy Sciences, the Delaware Research Partnership, and the DuPont Company.

Appendix

Neglecting secondary decomposition products, catalytic membranes can be benchmarked against the integrated yield of a non-selective, semi-batch membrane reactor that transports MTBE and its primary decomposition products from the reactor at the composition of the reactor. For example, assuming that the fugacity coefficients of the MTBE (1), isobutylene (2) and methanol (3) system are close to unity, the equilibrium conversion, x, for the closed volume above the membrane system at constant T and P is

$$KP = \frac{1-x}{x^2}$$

Nomenclature

K	equilibrium constant for MTBE synthesis (Pa^{-1})
P	pressure of MTBE (Pa)
p_0	initial MTBE pressure (Pa)
T	reaction temperature (°C)
x	equilibrium conversion of MTBE
x_1	mol fraction of MTBE above catalytic membrane
x_{int}	integral conversion of MTBE in semi-batch membrane reactor

or

$$x = \frac{-1+\sqrt{1+KP}}{2KP},$$

where K is the MTBE formation equilibrium constant. The mole fraction of MTBE at equilibrium in this closed volume is then:

$$x_1 = \frac{1-x}{1+x} = \frac{2KP+1-\sqrt{1+4KP}}{2KP-1+\sqrt{1+4KP}}.$$

If a non-selective membrane barrier exists at the boundary of the enclosure, this membrane would transport the gas mixture from the reactor with a flux having a composition of the enclosure. Likewise, the integral conversion can be defined as the total amount of reactant converted to decomposition products as the reactor depletes the enclosure from an initial charge, down to zero-charge pressure. Because the instantaneous conversion (at a particular T and P) increases with decreasing pressure, the condition where the gas mixture is at all times in equilibrium as it is depleted from the reactor enclosure yields the maximum integral conversion. In this case, the integrated conversion of the reactor from an initial MTBE charge of $P = p_0$ to $P = 0$ is

$$\begin{aligned} x_{int} &= 1 - \frac{1}{p_0}\int_{p_0}^{0}\left(\frac{2KP+1-\sqrt{1+4KP}}{2KP-1+\sqrt{1+4KP}}\right)\mathrm{d}P \\ &= 1 - \frac{1}{Kp_0}\left[2\sqrt{1+4Kp_0} - 2 - Kp_0 \right. \\ &\qquad \left. + 3\ln\left(\frac{4(3-\sqrt{1+4Kp_0})}{(Kp_0-2)(3+\sqrt{1+4Kp_0})}\right)\right]. \quad \text{(A.1)} \end{aligned}$$

The integrated conversion of this idealized reactor decreases with increasing charge pressure as expected.

References

[1] J.N. Armor, Appl. Catal. 49 (1989) 1.
[2] J.N. Armor, Chemtech 22 (1992) 557.
[3] G. Saracco, H. Neomagus, G.F. Versteeg and W.P.M. van Swaaij, Chem. Eng. Sci. 54 (1999) 1997.
[4] J.N. Armor, Catal. Today 25 (1995) 199.
[5] M.J. Alfonso, A. Julbe, D. Farrusseng, M. Menendez and J. Santamaria, Chem. Eng. Sci. 54 (1999) 1265.
[6] J.M. van de Graaf, M. Zwiep, F. Kapteijn and J.A. Moulijn, Appl. Catal. A 178 (1999) 225.
[7] J.M. van de Graaf, M. Zwiep, F. Kapteijn and J.A. Moulijn, Chem. Eng. Sci. 54 (1999) 1441.
[8] N. Itoh and K. Haraya, Catal. Today 56 (2000) 103.
[9] M. Strano and H.C. Foley, AIChE J. 47 (2001), in press.

[10] M. Acharya, M.S. Strano, J. Mathews, S.J.L. Billinge, S.S. and H.C. Foley, Phil. Mag. B 79 (1999) 1499.
[11] H.C. Foley, Abstr. Pap. Am. Chem. Soc. 211 (1996) 2.
[12] R.K. Mariwala and H.C. Foley, Ind. Eng. Chem. Res. 33 (1994) 2314.
[13] M. Acharya, B.A. Raich, H.C. Foley, M.P. Harold and J.J. Lerou, Ind. Eng. Chem. Res. 36 (1997) 2924.
[14] M. Acharya and H.C. Foley, J. Membr. Sci. 161 (1999) 1.
[15] M.B. Shiflett and H.C. Foley, Science 285 (1999) 1902.
[16] T. Okuhara, N. Mizuno and M. Misono, Adv. Catal. 41 (1996) 113.
[17] M. Misono, Catal. Rev. Sci. Eng. 29 (1987) 269.
[18] Y. Izumi and K. Urabe, Chem. Lett. (1981) 663.
[19] M.A. Schwegler, P. Vinke, M. van der Eijk and H. van Bekkum, Appl. Catal. A 80 (1992) 41.
[20] J.K. Lee, I.K. Song and W.Y. Lee, Catal. Lett. 29 (1994) 241.
[21] J.K. Lee, I.K. Song and W.Y. Lee, Catal. Today 25 (1995) 345.
[22] M.S. Strano and H.C. Foley, AIChE J. 46 (2000) 651.
[23] I.V. Kozhevnikov, A. Sinnema, R. Jansen and H. van Bekkum, Catal. Lett. 27 (1994) 187.
[24] A. Ghanbaari-Siahkali, A. Philippou, J. Dwyer and M.W. Anderson, Appl. Catal. A 192 (2000) 57.
[25] M.S. Strano and H.C. Foley, Carbon (2001), submitted.
[26] M.S. Kaba, M.A. Barteau, W.Y. Lee and I.K. Song, Appl. Catal. A 194–195 (2000) 129.
[27] S.G. Lias, J.F. Liebman, R.D. Levin and S.A. Kafafi, *NIST Standard Reference Database 25* (National Institute of Standards and Technology, Washington, 1994).
[28] J.S. Vaughan, C.T. O'Connor and J. Fletcher, J. Catal. 147 (1994) 441.
[29] M. Lisal, W.R. Smith and I. Nezbeda, AIChE 46 (2000) 866.